Combustion and Flame 266 (2024) 113516

Contents lists available at ScienceDirect

Combustion and Flame

journal homepage: www.sciencedirect.com/journal/combustion-and-flame

Effect of inter-jet spacing on soot formation in the direct injection diesel combustion process

T. Montiel [a], R. Payri [b], P. Martí-Aldaraví [b,*], M. Carreres [b]

[a] Symanto Spain S.L.U., Calle de la Reina, 12, Valencia, 46011, Comunitat Valenciana, Spain
[b] CMT, Universitat Politècnica de València, Camino de Vera, s/n, Valencia, 46022, Comunitat Valenciana, Spain

ARTICLE INFO

Keywords:
Soot
Optical thickness
Inter-jet spacing
Diesel combustion
Engine-like conditions

ABSTRACT

Last events taking into account the growing enviromental awareness motivated the automotive industry community to further improve internal combustion engines (ICE), which should remain relevant for the foreseeable future. Pollutant emission mechanisms in the last strategies followed to reduce fuel consumption, such as the use of smaller diameters multi-hole injector nozzles, need to be investigated. The effect of jet-spacing in soot formation is yet unclear, this being the goal of the present work. A high-pressure and high-temperature vessel with large optical accesses is employed. Two diesel injectors with six outlet orifices were used. The only difference between them is the geometric distribution of the outlet holes, so 30°, 36°, 45° of jet spacing are compared to an isolated spray. The Diffuse back-illumination (DBI) technique is implemented to compute the soot optical thickness and mass. For that, a novel window was designed together with the injector holder for proper optical access. A wide test matrix varying ambient temperature, density and oxygen concentration as well as injection pressure was selected. The spray configuration with closer sprays (30° and 36°) had higher optical thickness and peak soot mass when compared to the isolated spray probably due to local effects of hot gases re-entrainment. The impact of the inter-jet spacing was smaller under boundary conditions promoting soot formation.

Novelty and significance

Most of the research studies about the inter-jet spacing have been carried out in engines with limited optical access. In turn, fundamental and focused works, performed in controlled environments inside high-pressure and high-temperature test chambers, have not deeply analyzed combustion emissions such as soot. The main novelty and significance of this work is precisely this analysis. The DBI technique with strong and fast LEDs is applied to assess the temporal evolution of soot formation on the injection event. Light extinction is used to obtain the soot extinction coefficient across the soot cloud of direct injection diesel sprays, which is related to the soot mass produced. Three inter-jet spacing configurations are analyzed and compared to the performance of a single isolated spray. These new results will complete the study of the effect of the jet-to-jet separation on the combustion process available in the literature.

1. Introduction

The growing environmental awareness of last decades has led to the creation of emissions and fuel economy legislation that have been increasingly restrictive throughout the years [1]. These events have motivated the industry and the research community to continuously search for improvements in multiple areas of the internal combustion engine (ICE), leading to a notable increase in their efficiency [2,3]. Even though their usage is currently decreasing for ground transportation, there are several factors as to why the ICE should remain highly relevant for the foreseeable future: they have become highly efficient in terms of pollutant emissions [4], they still are key to maintain the current standard of living, and the alternatives to replace them for light and heavy-duty vehicles face environmental and economic unresolved challenges. It is then reasonable that oil remains as the highest source of energy consumption [4] for at least several years.

Regarding the diesel engines, a main area of study has been the direct spray injection process, as the air/fuel mixing process is a critical factor to reduce pollutant emissions during the combustion development [5,6]. On this matter, numerous techniques have been analyzed and implemented, such as increasing the injection pressure

* Corresponding author.
E-mail address: pedmar15@mot.upv.es (P. Martí-Aldaraví).

https://doi.org/10.1016/j.combustflame.2024.113516
Received 6 September 2023; Received in revised form 25 April 2024; Accepted 15 May 2024
Available online 24 May 2024

[7], employing multiple injection strategies [8], improving the nozzle geometry [9], and so on. A strategy of particular interest for this work is the implementation of injectors with multiple outlet-orifices in the nozzle [10]. In this sense, increasing the number of outlet holes has allowed to have smaller diameters, leading to smaller droplet sizes and so enlarging the liquid-gas contact surface. This generally leads to more homogeneous mixtures, enhancing the combustion event. Nevertheless, increasing the number of holes leads to a reduction in the space available for each jet to independently develop without interacting with the neighbor sprays. Then, this strategy represents a trade-off between improving the air entrainment through smaller orifice diameters and providing a larger volume of air between sprays. In this sense, as the sprays come closer to each other, jet-to-jet interaction could significantly affect the combustion process with implications not entirely defined yet [11,12].

Some of the research works in this area were performed, on the one hand, in real diesel engines [13,14] in which minor modifications were done to gain optical access to the combustion chamber. On the other hand, fundamental analysis through optically accessible test rigs with controlled boundary conditions [15] has eased the implementation of optical diagnostics allowing to perform high-fidelity experiments focusing on specific parameters to have a greater understanding of the topic of interest [16–18]. This type of fundamental analysis on multi-hole injectors is not as developed as with isolated sprays, explaining why the interaction between jets and its effect on the combustion process has not been entirely defined. Rusly et al. [14], in a small-bore optical diesel engine, found that for narrow inter-jet spacing the impact of spray interaction on the lift-off length (LoL) and natural soot luminosity is more significant than the effect of the re-entrainment from the spray-wall interaction. Similar results were found by Le at al. [19]. They suggested increasing the inter-jet spacing to reduce the high-temperature gas re-entrainment and shorten the LoL. Chartier et al. [13] measured the influence of jet-to-jet interactions on the LoL, observing that burned gases from neighbor jets entrain the lift-off region, shortening LoL, phenomenon that gained importance when reducing the inter-jet spacing. These authors also found a strong interaction between the chamber gas temperature and the spacing between jets, probably due to the local gas temperature being dominated by the re-entrained burned gas in close sprays cases. Lequien et al. [20] noticed a shorter liquid length penetration for the spray with maximum inter-jet spacing with hot gas reservoirs formed by the combustion products near the lift-off area not strongly affecting the liquid length, trend attributed to the cooling effect of the surrounding jets. Polonowski et al. [21], in turn, found that low jet spacing could lead to “proximity coupling” between adjacent sprays in which several mechanisms (mixing rates modified by different velocity fields in interacting versus isolated jets upstream of the LoL, heat and radicals exchange between plumes at and downstream of the LoL, plumes with short LoL sequentially shortening the LoL of surrounding plumes) snowball towards a reduction in LoL compared to that of an isolated jet. Concerning the different velocity fields in interacting versus isolated jets, Malbec et al. [22] observed through PIV in a high-pressure test rig a faster upstream motion of the entrained gas between plumes when reducing jet spacing. Fuyuto et al. [23], in fact, provided imaging of the upstream flow of entrained hot product gases in an optical engine that also allow justifying a reduction in LoL for low jet spacings. Bazyn and Koci [24] and Payri et al. [25] also analyzed the LoL for several jet spacing configuration but in an optically accessible test rig, reporting that for spacing values above the threshold level of 36° of inter-jet spacing, sprays had a behavior similar to that of a single jet. Payri et al. [25] even provided a novel statistical regression for the LoL which accounted for the effect of the proximity between sprays.

As previously commented, most of the research studies about the inter-jet spacing have been carried out in engines with limited optical access, whereas fundamental and focused works, performed in controlled environments inside high-pressure and high-temperature test chambers, have not deeply analyzed combustion emissions such as soot. Furthermore, instead of the well known Laser Extinction Method (providing only a single image per injection event) [26,27], Diffuse Back-Illumination (DBI) technique with strong and fast light-emitting diodes (LEDs) is applied to assess the temporal evolution of soot formation on the injection event. Light extinction is used to obtain the soot extinction coefficient across the soot cloud, which is related to the soot mass produced. Three inter-jet spacing configurations are analyzed and compared to the performance of a single isolated spray. These new results will complete the study of the effect of the jet-to-jet separation on the combustion process available in the literature [25], in addition to serve as a valuable database to validate models through Computational Fluid Dynamics (CFD), a crucial tool to reduce testing times and production costs.

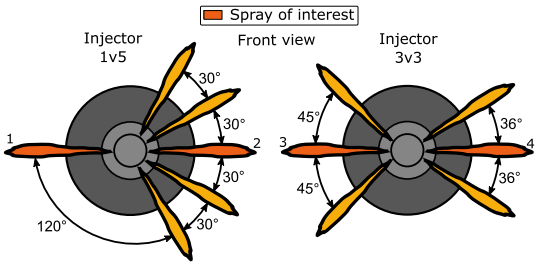

Fig. 1. Front-view sketch of the geometric distribution of the outlet holes. The sprays of interest are numbered from 1 to 4 and highlighted in dark orange. (For interpretation of the references to color in this figure legend, the reader is referred to the web version of this article.)

2. Materials and methods

2.1. Fuel delivery system and diesel injectors

Standard diesel fuel [28] is retrieved from a tank, purged of air and filtered to remove particles and impurities. A CP3 pump raises the pressure of a pressure-regulated common rail (of 22 cm^3 of volume and 28 cm long), which is directly connected to the injector through a high-pressure line. The excess of fuel coming out of the pump and the common-rail is sent back to the purger and the tank after passing through a heat exchanger where its temperature is controlled. Coolant is continuously flowing through the injector holder on the test rig, with a constant temperature of 363 K. An aluminum shield nozzle holder is used in combination with the novel injector port described in Section 2.3 As investigated in a previous work by the authors [29], this system allows the injector tip temperature to remain quite insensitive to chamber temperature. This fact, together with the large residence time of the fuel within the injector in the measurements (injection frequency of 0.25 Hz), gives confidence that the injected fuel temperature is very close to the injector holder coolant temperature (±10 K), so the results of the investigation are not biased by fuel temperature effects.

As in previous related studies [25], two diesel injectors with six outlet orifices were used. They were manufactured by Continental specifically to study the influence of the inter-jet spacing, with identical design (nominal orifice outlet diameter of 90 μm, K-factor of 5.1, 7.7% of hydro-erosion, opening angle of 150°, and maximum injection pressure of 250 MPa) except for the geometric distribution of the outlet holes of each nozzle. A sketch of the jet distribution of both injectors is shown in Fig. 1. Specifically, the first injector (1v5) allowed the study of the development of an isolated spray and sprays with an inter-jet spacing of 30° during the same injection event. The second injector (3v3) had two additional orifice distributions, so a total of three inter-jet spacing configurations (30°, 36°, and 45°) can be compared to the performance of the isolated spray for the same boundary conditions. Rate of injection (ROI) and rate of momentum (ROM) of these two

Table 1
Boundary conditions for the soot-DBI experiments.

Parameter	Value
Chamber gas temperature [K]	800 – 900 – 1000
Chamber gas density [kg/m^3]	15.2 – 22.8 – 30.4
Chamber gas oxygen concentration [%$_{vol.}$]	13 – 17 – 21
Fuel injection pressure [MPa]	100 – 150 – 200

injectors were measured to hydraulically characterize the sprays as a function of the injection conditions (injection pressure and discharge pressure) [30,31]. In this regard, all sprays exhibited a similar performance, the influence of the pressure drop being more noticeable than the influence of the individual spray of interest itself. An average discharge coefficient $C_d = 0.90$ and an average momentum coefficient $C_M = 0.75$ were found, with standard deviations among sprays of ± 0.01 in both cases.

2.2. Test rig and test matrix

An optically accessible high-pressure and high-temperature constant pressure flow combustion chamber was employed in this study. This chamber is able to reproduce real engine thermodynamic conditions up to temperatures and pressures of 1100 K and 15 MPa, respectively. Additionally, the test rig can maintain nearly quiescent and steady conditions within the chamber with constantly renovated ambient gas. A full description of this test rig can be found in a previous work of Payri et al. [27]. As sketched in Fig. 2(b), the chamber includes a frontal view to record the injection event of multi-orifice injectors (the ones used in this study), and two other lateral windows.

The boundary conditions employed throughout the experimental campaign are summarized in Table 1. Three different values for ambient gas temperature and density (chamber pressure) are selected. Injection pressure is varied also in three levels. The oxygen concentration of the chamber air was also modified. This parameter is known to alter both the soot distribution and the amount of soot produced [32], and will serve to simulate exhaust gas recirculation (EGR) conditions in the engine. The total of the 81 boundary conditions are tested for each of the 4 jet-spacing situations shown in Fig. 1.

To reduce measurement errors and uncertainties, 15 injection repetitions were measured for each of the 81 different boundary conditions (Table 1). Results of all repetitions were averaged, and the relative standard deviation was obtained. Even though deviation data is omitted from most plots and tables presented in the results section for clarity and readability, the average deviation found was 3.3%.

2.3. Optical setup: soot-DBI technique

In recent years, applying the DBI technique has become increasingly popular, specially with the appearance of LED, which can be configured to emit strong light intensity for a brief period (in the order of nanoseconds), even smaller than the shorter exposure time per frame of a high-speed camera. Thus, the light exposure per frame can be governed by the LED pulse, and the images obtained can be of a much sharper resolution than with other continuous light sources [33,34]. DBI requires a cleared line of sight from the back to the front of the spray, which is particularly complex for multi-orifice injectors. To fulfill this requirement, a novel window was designed and manufactured. The injector holder and an optical access for the illumination were placed in the same piece, shown in Fig. 2(a). Additionally, various pieces of the injector holder were also redesigned to allow the rotation of the injector. Thus, it was possible to align the spray of interest without having to dismount the injector, consequently allowing to deploy part of the optical setup behind this new window.

As seen in Fig. 2(b), the light originating from the red LED (light wavelength of 660 nm, pulse duration of 900 ns) was properly directed with a Fresnel lens and then passed through an engineered diffuser (EDC-20 by RPC Photonics), which created a diffused Lambertian intensity profile [35]. Afterward, the light went through the soot cloud and into the camera, capturing the attenuation produced. Images were obtained at a frequency of 36,000 fps and an image resolution of 768 × 304 pixels, with 6.45 pixels corresponding to 1 mm. The Photron Nova S9 camera was employed, with its sensor enhanced by the manufacturer to inhibit image ghosting [36].

Some considerations or limitations appeared as a trade-off to the complexity of the setup. In particular, the following two restraints should be considered in the analysis of the results:

- Limited field of view of the spray: the injector and the optical window had to be mounted in the same piece, complying with the structural limitations and the space available in the test rig. The resulting field of view started at 30 mm and ended at 85 mm from the injector nozzle. Consequently, soot formation could not be properly addressed when boundary conditions promoted faster premixed combustion near the nozzle (higher gas chamber temperature, density, and oxygen concentration).
- Fixed optical setup: the LED intensity and the camera diaphragm aperture were kept constant during the experimental campaign, limiting the maximum light intensity that could be employed. Thus, the LED power was not always enough to effectively measure a soot extinction coefficient in the boundary conditions that had the highest-density soot clouds, as in such conditions soot can completely obstruct the path of the light beams from the soot cloud to the camera [37]. Those cases resulted in a distorted measured soot extinction coefficient, where a theoretical maximum measurable value of the particular setup (further details are given in Section 2.4) was reached where the soot extinction coefficient would actually be higher.

2.4. Image post-processing and soot mass calculation

The fast-response LED allows capturing the temporal evolution of soot, although limited to the image's dynamic range. Particularly, during each image acquisition event, the high-speed camera records a frame with the LED-on and the next one with the LED-off. The LED-on frame details the amount of light coming from the LED plus the natural luminosity of the spray, while the LED-off frame only depicts the natural luminosity of the spray. Nevertheless, these two frames are not obtained at the exact same time, so a two-frame motion interpolation process based on polynomial expansion was employed. In particular, it estimates the direction and speed of the optical flow from the previous frame to the current one, using Gunnar Farneback's motion estimator algorithm [38]. Thus, an intermediate frame can be recreated so the LED-on and LED-off frames can be compared for the same instant.

The natural luminosity of the spray, the LED-off frame, is subtracted to the frame with the LED-on frame in order to obtain the real light attenuation. Then, a qualitative measurement of the soot concentration can be calculated through Eq. (1) (Beer–Lambert Equation [39]), where I_{on} represents the pixel intensity with the LED-on, I_{off} the intensity with the LED-off, I_o the LED-on intensity before the start of the injection, K the soot dimensional extinction coefficient, and L the light beam path length through the soot cloud. The product KL then represents the soot extinction coefficient across the soot cloud and is directly related to the soot produced. This process is graphically exemplified in Fig. 3.

$$\frac{I_{on} - I_{off}}{I_o} = e^{-KL} \tag{1}$$

The maximum measurable KL mentioned in Section 2.3 occurs when the soot cloud completely attenuates the LED light. In such conditions, there is no transmitted light across the soot cloud. Then, the light captured by the camera in the spray area only comes from

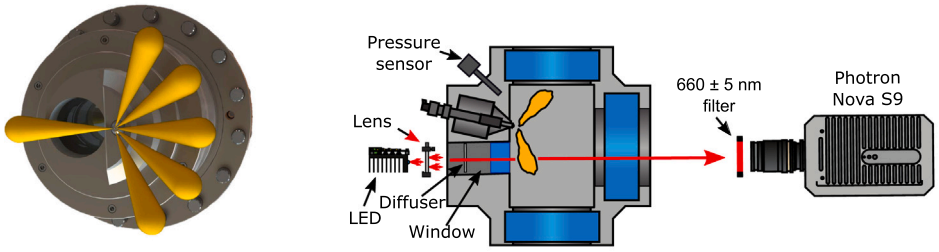

(a) Novel window and injector holder. (b) Optical setup.

Fig. 2. Sketch of the soot-DBI experimental test rig for multi-hole injectors.

the natural luminosity of the spray, both in the LED-on and LED-off frames. In that case, the term $I_{on} - I_{off}$ of Eq. (1) results in a black image. The maximum measurable KL can then be computed through Eq. (2), where I_{min} is the minimum transmitted intensity, which comes from the camera shading uncertainty and is obtained averaging the I_{off} frames before the start of injection.

$$\frac{I_{min}}{I_o} = e^{-KL_{max}} \tag{2}$$

Following the procedure described next, a proper qualitative measurement of the amount of soot produced during the entire injection can be given in a single image:

- The pixel intensity along the vertical (cross-sectional) axis is added up for each axial distance from the nozzle. This axis length is set to sum all values of a single spray under all test conditions, avoiding neighbor sprays even at the smallest inter-space distance. An example of a cross-sectional axis at 60 mm of axial distance is shown in the left hand side plot of Fig. 4, which represents one frame of the KL profile.
- The resulting value is plotted in the KL map, the right hand side contour plot of Fig. 4. The red dot in the plot points the value at 60 mm and 2.7 ms used as an example.
- The sum is repeated for every axial distance. The result at 2.7 ms shown on the left plot of Fig. 4 provides the distribution along the white line plotted on the right plot of Fig. 4.
- This process is done for every time step of the injection, computing the KL map for the entire event. The final result is a contour plot such as the one shown at the right-hand side plot of Fig. 4.

Through the small particle Mie theory, the dimensional extinction coefficient (K) is related to the soot volume fraction (f_v) along the line of sight of the extinction path [40] as shown in Eq. (3). There, L represents the soot path length, λ is the wavelength of the light (660 nm in this work), and k_e is the dimensionless optical extinction coefficient. This coefficient is computed with Eq. (4) following the Rayleigh–Debye–Gans methodology [26,27,41], where α_{sa} is the scattering-to-absorption ratio, and n_s refers to the complex refractive index of the soot particles. Both α_{sa} and n_s were extracted from the works of Köylü et al. [41] and Manin et al. [26], so $k_e = 7.27$ was determined for the LED wavelength of 660 nm.

$$f_v = \frac{K\,\lambda}{k_e} \rightarrow \int_0^L f_v \,\mathrm{d}l = \frac{K\,L\,\lambda}{k_e} \tag{3}$$

$$k_e = \left(1 + \alpha_{sa}\right)\, 6\pi\, \Im\left[\frac{n_s^2 - 1}{n_s^2 + 2}\right] \tag{4}$$

The soot mass along the line of sight of each pixel can be expressed as in Eq. (5), where A_{pixel} represents the area in the light of sight projected onto the camera. This pixel area is computed from the pixel-mm image ratio (6.45 px/mm in this work), and the soot density was assumed as 1.8 g/cm^3 [40].

$$m_{soot} = \rho_{soot}\, V_{soot} = \rho_{soot}\, f_v\, V \rightarrow m_{soot,pixel}$$

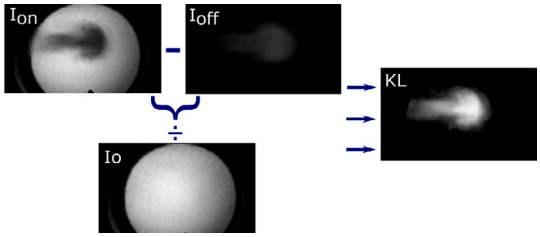

Fig. 3. KL profile calculation process (Eq. (1)). Example at 2.7 ms aSOI for a gas temperature of 900 K, gas density of 22.8 kg/m^3, injection pressure of 150 MPa, oxygen concentration of 17%, and inter-jet spacing of 36°.

$$= \rho_{soot} \int f_v\, A_{pixel}\, dl = \rho_{soot}\, \frac{K\,L\,\lambda}{k_e}\, A_{pixel} \tag{5}$$

Then, the soot mass of a particular time step (within the optical range of the visualization window) is the sum of all pixel specific values over the entire spray in the image. Nonetheless, this methodology requires wariness due to the considerable uncertainties associated with the soot optical properties (both α_{sa} and n_s) and the assumption of constant soot density. Even so, a clearer assessment of the observed trends can be made, and results still provide useful information for CFD modeling [42].

3. Results

Regarding the soot formation, the chamber temperature is one of the parameters with the most significant influence on the produced soot [35]. Therefore, the KL results will be grouped in three sections corresponding to each of the values of chamber temperature tested, from low to high: 800 K, 900 K, and 1000 K. Within each temperature group, data is presented increasing gas chamber density, analyzing the influence of every boundary condition.

Throughout the measurements, the soot cloud location got closer to the nozzle as the oxygen concentration increased, altering the amount of soot inside the field of view. Consequently, no definite quantitative or qualitative assessment could be made on this parameter. Nevertheless, altering oxygen concentration served to obtain more test points inside the field of view. Specifically, the chamber density and temperature affected the ignition location as well, so changing the oxygen concentration worked to compensate for these effects and have more test points inside the field of view at every temperature and gas density. Thus, for each combination of boundary conditions, the oxygen concentration for which the ignition and soot had the greater development within the field of view will be presented in order to improve readability.

3.1. Soot maps under 800 K

For low gas chamber density conditions (15.2 kg/m^3), none or negligible soot (cross-sectional $KL < 20$) was found. Intermediate density

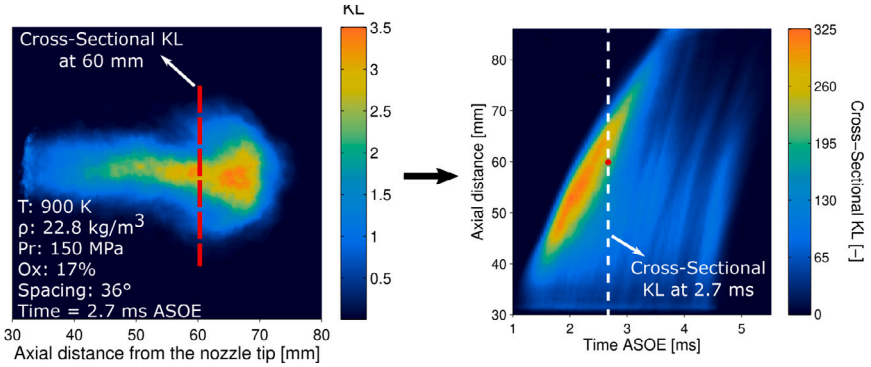

Fig. 4. Computation of the KL map.

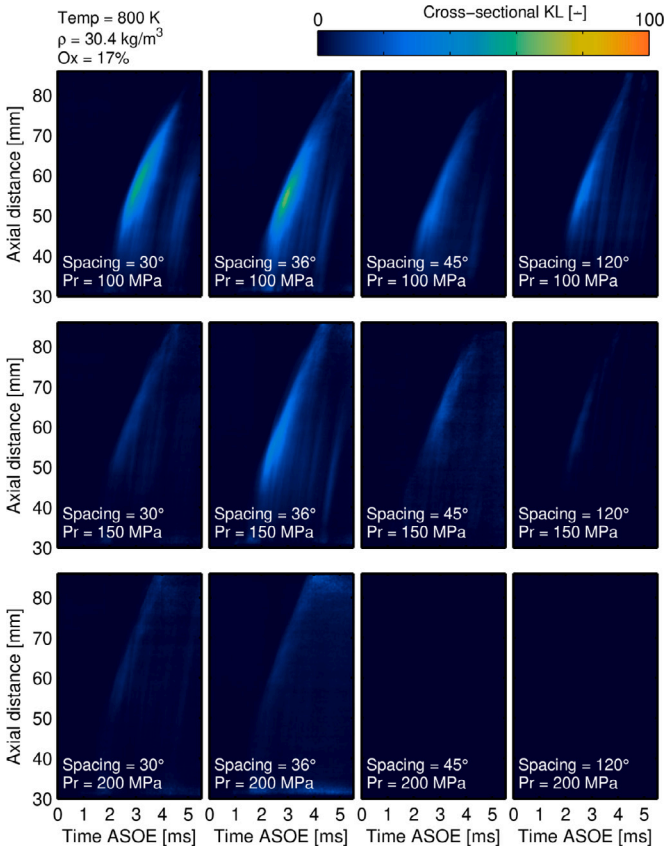

Fig. 5. KL maps for every inter-jet spacing configuration and injection pressure at 800 K of gas chamber temperature, 30.4 kg/m^3 of density, and 17% of oxygen concentration boundary conditions.

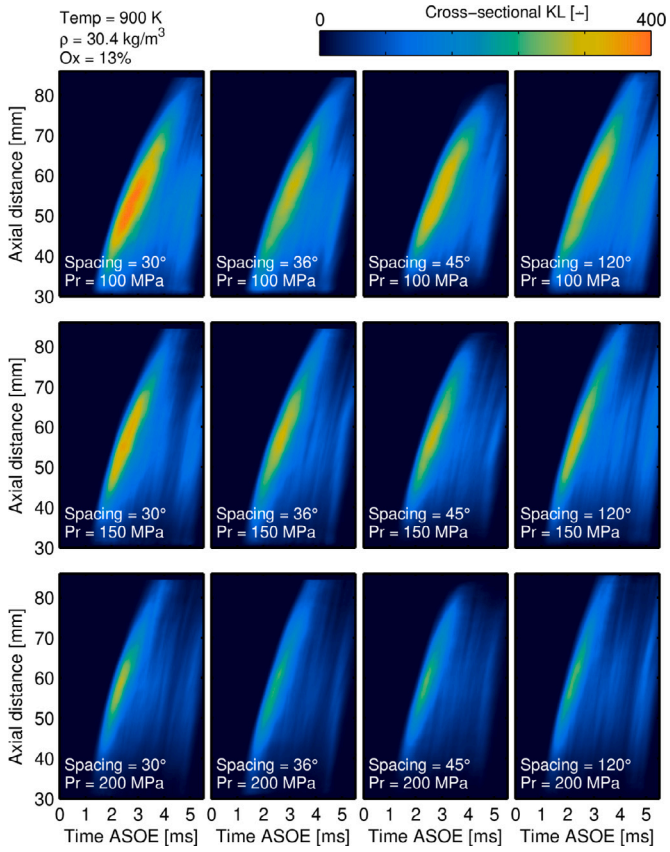

Fig. 6. KL maps for every inter-jet spacing configuration and injection pressure at 900 K of gas chamber temperature, 30.4 kg/m^3 of density, and 13% of oxygen concentration boundary conditions.

values (22.8 kg/m^3) led to soot particles appearing on the field of view, although these appearances were unstable due to still poor combustion. Fig. 5 depicts the cross-sectional KL maps for the highest gas chamber density (30.4 kg/m^3) boundary conditions. The appearance of soot became more stable and noticeable. None or small amount of soot was found for the isolated jet (spacing of 120°). In contrast, the sprays with a close distance to their neighbor jets, specially under the 30° and 36° inter-jet spacing configurations, had denser soot-cloud in terms of optical thickness (KL).

3.2. *Soot maps under* 900 K

Increasing the gas chamber temperature shortens both ignition delay and lift-off length [43] particular data for these sprays from a previous work [25] is summarized in Appendix, resulting in richer air-fuel mixture ratios near the lift-off area, which promote soot production [44]. Regarding the injection pressure, it reduced the soot formation given that the fuel-air mixing rate is enhanced and the lift-off lengthened (recall Appendix). Thus, combustion happens under leaner equivalence ratio conditions, partially inhibiting soot formation. And again, enlarging the gas chamber density has a direct effect boosting soot formation [27]. These trends are clearly shown in the cross-sectional KL maps of Fig. 6.

Regarding the inter-jet spacing, Fig. 6 shows that the configurations with close spacing between sprays generally have denser soot clouds (a pattern continuously observed throughout the measurements campaign). This trend is both in line with literature observations [21] and previously obtained results on LoL (Appendix), in which the closely

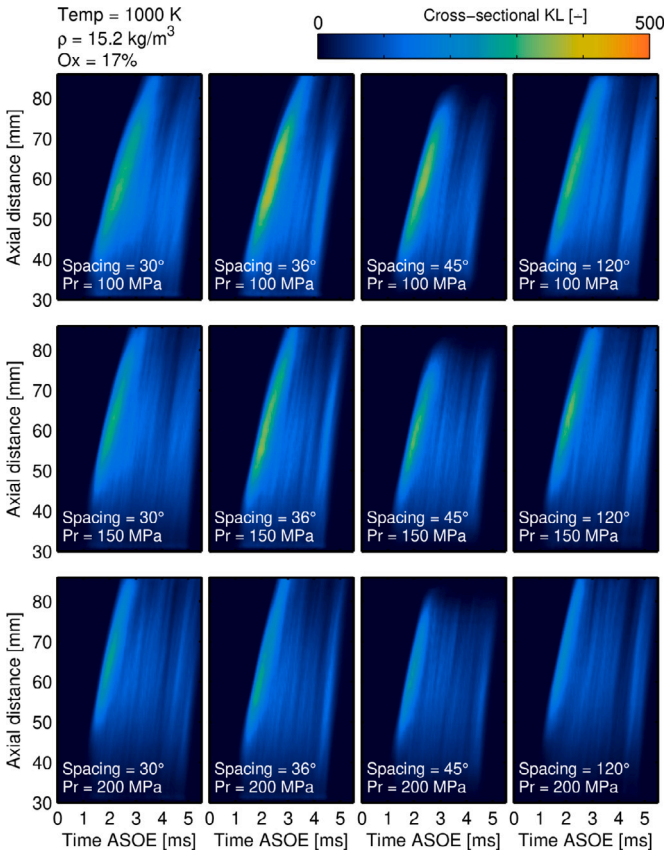

Fig. 7. KL maps for every inter-jet spacing configuration and injection pressure at 1000 K of gas chamber temperature, 15.2 kg/m^3 of density, and 17% of oxygen concentration boundary conditions.

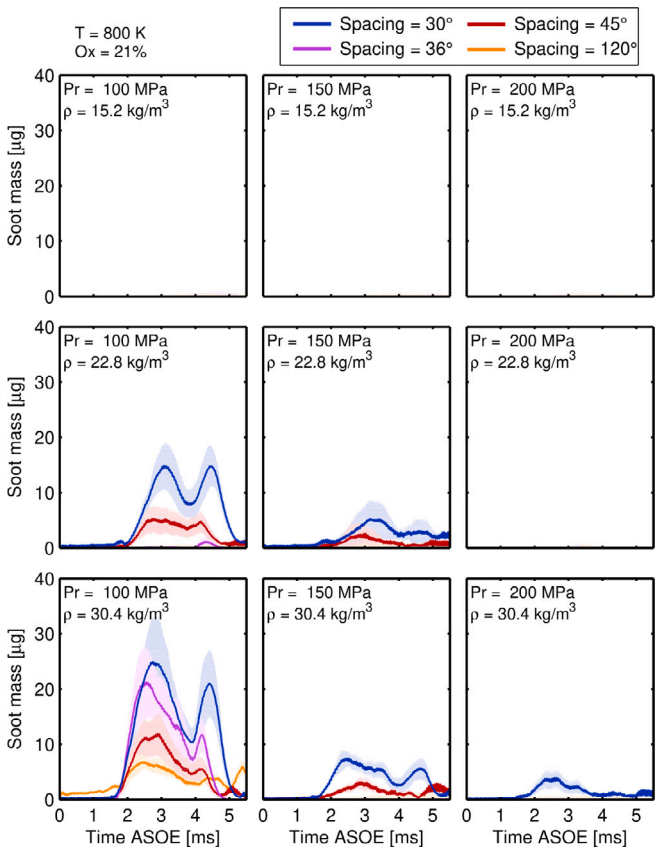

Fig. 8. Temporal evolution of the soot mass captured within the field of view for every inter-jet spacing configuration, injection pressure, and gas chamber density with 800 K of gas chamber temperature and 21% of oxygen concentration.

spaced jets had a shorter lift-off length. This shorter LoL can be explained due to hot gases re-entrainment [13,14,19], which can be in turn explained by a faster upstream gas motion [22] or backward flow of hot burned gases between plumes [23]. The LoL shortening would lead to the combustion occurring under richer mixture conditions, suitable for soot formation [21]. Moreover, this contrast increased when lowering the rail pressure. Thus, the impact of the inter-jet spacing could be more significant under the poor atomization and mixing development inherent to low injection pressures.

3.3. Soot maps under 1000 K

The direct influence of the chamber temperature on soot formation emerged again with the appearance of the densest soot clouds of the test campaign. Moreover, the results under various boundary conditions could not be analyzed because KL reached the maximum measurable magnitude from Eq. (2). Specifically, this was the case of test points with oxygen concentration of 13% (the reduction of oxygen availability results in denser soot clouds, since the oxidation process is inhibited [35]) and the highest gas chamber density (30.4 kg/m^3), in which, in addition, the sprays mostly ignited and developed before entering the field of view.

In comparison with the previous values studied, Fig. 7 depicts that the influence of inter-jet spacing on soot formation was less predominant under 1000 K of gas chamber temperature. Plausibly, the influence of the high temperature could overall be overcoming the local effect that the interaction between the sprays can have. Nonetheless, the sprays with closely spaced neighbor jets still showed slightly higher soot formation.

3.4. Soot formation

Figs. 8 and 9 (selected boundary conditions where KL did not reach the maximum measurable values according to Eq. (2)) depict the soot mass obtained within the optical access. The shade throughout each curve represents the 95% confidence interval of the test point. Although the computation methodology presents some constraints (details in Section 2.3), these figures serve as a complement to the results observed in previous sections, as they provide a comparison for every inter-jet spacing on a given boundary condition in the same plot.

The sprays with close neighbor jets typically formed more soot than an isolated spray. Moreover, soot only appeared within sprays with neighbor jets in some boundary conditions. At 800 K, the soot formation was unstable from cycle to cycle, as reflected by the wider confidence interval compared to higher temperature test points.

Parametric variations of the boundary conditions showed similar influences on the soot formation to those already explained in previous sections and in accordance with previous studies [27,35]. Increasing the gas chamber pressure, the soot formation notably increased. Increasing the injection pressure reduced the soot formation. Also, higher gas chamber densities increased the soot appearance, although this trend was not always noticeable at 30.4 kg/m^3 since the sprays typically ignited before entering the field of view. A similar limitation appeared when increasing the oxygen concentration.

Regarding the inter-jet spacing, the sprays with an inter-jet spacing of 30° and 36° frequently produced more soot than the others. The jet with a spacing of 45° reported an intermediate behavior, with its soot production being typically more similar to that of the isolated spray. Nevertheless, the trend is not monotonic (see for instance Fig. 9). Under 800 K (Fig. 5) and 1000 K (Fig. 7) of ambient temperature, a spacing

Table 2
Lift-off length data for selected conditions (Ox = 21%$_{vol.}$, $\rho = 15.2\,kg/m^3$).
Source: Adapted from [25].

				Lift-Off length [mm]				Ignition delay [ms]			
				Spacing				Spacing			
				30°	36°	45°	120°	30°	36°	45°	120°
T [K]	800	Pr [MPa]	100	37.9	45.0	47.3	47.5	2.31	2.23	2.21	2.24
			150	41.6	50.5	50.7	51.9	–	–	–	–
			200	44.8	57.1	56.6	57.5	–	–	–	–
	900	Pr [MPa]	100	13.9	17.6	19.0	19.9	0.88	0.86	0.83	0.88
			150	17.0	21.2	22.2	23.4	–	–	–	–
			200	19.2	23.7	26.0	26.8	–	–	–	–
	1000	Pr [MPa]	100	10.7	10.5	13.9	14.6	0.59	0.58	0.56	0.54
			150	11.5	12.1	14.8	16.5	0.49	0.45	0.44	0.47
			200	12.8	13.4	15.2	16.9	0.41	0.40	0.40	0.42

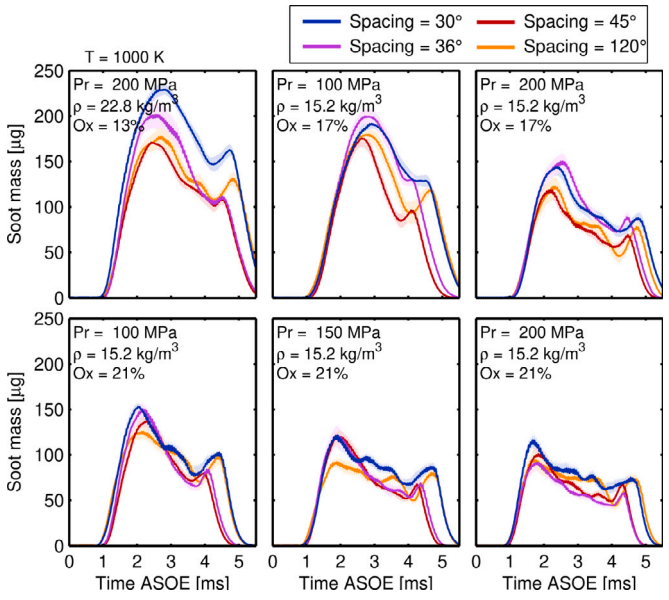

Fig. 9. Temporal evolution of the soot mass captured within the field of view for every inter-jet spacing configuration, injection pressure, and gas chamber density which could be properly measured with 1000 K of gas chamber temperature.

of 36° generates more soot than the spacing of 30°, while for 900 K (Fig. 6) it is the spacing of 30° the configuration that reports more soot. This means that the influence of other parameters such as the ambient temperature or the injection pressure could be overcoming the local effects occurring between the sprays in nozzle configurations with close sprays. On the other hand, the influence of the inter-jet spacing generally decreased as the air/fuel mixing conditions were enhanced, that is, as the gas chamber density and injection pressure increased.

4. Conclusions

The present article discusses the results of the spray performance and soot formation for multiple inter-jet spacing configurations in reactive conditions. The experiments were done in a high-pressure and high-temperature test rig with wide optical access. The optical technique was the diffused back-illumination, used to compute the optical thickness KL of the spray, a direct indicator of soot production.

To do so, a novel optical window was fabricated to apply the DBI technique on multi-hole injectors. The field of view was consequently restrained, starting at 30 mm from the nozzle and ending at 85 mm. Therefore, the influence of the inter-jet spacing could not be properly addressed when the ignition occurred before the spray entered the field of view. Lastly, the soot mass observed within this field of view was computed by aggregating the KL at each time-step.

From the results shown here, the following conclusions were drawn:

- A wide test matrix was employed, collecting data on the boundary conditions at which the spray develops within the field of view. This information could help select an efficient test matrix in future works, saving time and additional expenses from experimental measurements.
- In general terms, the sprays with closely spaced neighbor jets (30° and 36°) had higher optical thickness KL and peak soot mass values for a given boundary condition when compared to the development of the isolated spray (spacing of 120°).
- These trends are in line with the previously obtained lift-off length results (summarized in Appendix), in which the closely spaced jets had a shorter lift-off length as described in the literature [13,14,19,21,23]. This shortening would deteriorate the air/fuel mixing before the onset combustion and, consequently, a richer mixture is ignited, suitable for soot appearance.
- On the other hand, the impact of the inter-jet spacing was smaller the more the boundary conditions promoted soot formation on their own, that is increasing the ambient density, ambient temperature, or reducing the injection pressure. The influence of these parameters on the soot formation could be overcoming the local effects occurring between the sprays.
- Additionally, the influence of the remaining boundary conditions on the soot formation was assessed. Firstly, increasing the rail pressure inhibited the soot formation, as combustion occurred with a leaner air/fuel mixture. On the other hand, enlarging the gas chamber density or temperature increased the soot formation, as the combustion developed under a higher equivalence ratio around the lift-off area. These trends follow previous analyses and serve to validate the consistency of the work done.

CRediT authorship contribution statement

T. Montiel: Conceptualization, Investigation, Methodology, Software. **R. Payri:** Funding acquisition, Project administration, Resources, Supervision. **P. Martí-Aldaraví:** Data curation, Formal analysis, Software, Writing – original draft. **M. Carreres:** Data curation, Formal analysis, Software, Writing – review & editing.

Declaration of competing interest

The authors declare that they have no known competing financial interests or personal relationships that could have appeared to influence the work reported in this paper.

Acknowledgments

This work has been partially funded by Spanish *Ministerio de Ciencia e Innovación* through SHYGAS project PID2021-125812OB-C21. Tomás Montiel was supported by a research grant from Generalitat Valenciana, Spain and the European Social Fund (reference ACIF/2018/122).

Appendix. Lift-off length and ignition delay data

Lift-off length (LoL) and ignition delay (ID) for the operating conditions corresponding to the chamber gas oxygen concentration of 21%$_{vol.}$ were reported in a previous work by the authors [25]. Results for selected conditions (chamber gas density of 15.2 kg/m^3) are summarized in Table 2 of this Appendix in order to facilitate the interpretation of the soot formation dataset.

References

[1] T.V. Johnson, Vehicular emissions in review, SAE J-Automot. Eng. 9 (2016) http://dx.doi.org/10.4271/2016-01-0919, 2012-01-0368.

[2] M. Lapuerta, Á. Ramos, D. Fernández-Rodríguez, I. González-García, High-pressure versus low-pressure exhaust gas recirculation in a Euro 6 diesel engine with lean-NOx trap: Effectiveness to reduce NOx emissions, Int. J. Engine Res. 20 (2019) 155–163, http://dx.doi.org/10.1177/1468087418817447.

[3] J. Claßen, S. Pischinger, S. Krysmon, S. Sterlepper, F. Dorscheidt, M. Doucet, C. Reuber, M. Görgen, J. Scharf, M. Nijs, S.C. Thewes, Statistically supported real driving emission calibration: Using cycle generation to provide vehicle-specific and statistically representative test scenarios for Euro 7, Int. J. Engine Res. 21 (2020) 1783–1799, http://dx.doi.org/10.1177/1468087420935221.

[4] T. Grigoratos, M. Gustafsson, O. Eriksson, G. Martini, Experimental investigation of tread wear and particle emission from tyres with different treadwear marking, Atmos. Environ. 182 (2018) 200–212, http://dx.doi.org/10.1016/j.atmosenv.2018.03.049.

[5] M.P.B. Musculus, P.C. Miles, L.M. Pickett, Conceptual models for partially premixed low-temperature diesel combustion, Prog. Energ. Combust. 39 (2013) 246–283, http://dx.doi.org/10.1016/j.pecs.2012.09.001.

[6] S. Han, J. Kim, C. Bae, Effect of air-fuel mixing quality on characteristics of conventional and low temperature diesel combustion, Appl. Energ. 119 (2014) 454–466, http://dx.doi.org/10.1016/j.apenergy.2013.12.045.

[7] X. Wang, Z. Huang, W. Zhang, O.A. Kuti, K. Nishida, O. Abiola, K. Nishida, Effects of ultra-high injection pressure and micro-hole nozzle on flame structure and soot formation of impinging diesel spray, Appl. Energ. 88 (2011) 1620–1628, http://dx.doi.org/10.1016/j.apenergy.2010.11.035.

[8] J. O'Connor, M.P.B. Musculus, L.M. Pickett, Effect of post injections on mixture preparation and unburned hydrocarbon emissions in a heavy-duty diesel engine, Combust. Flame 170 (2016) 111–123, http://dx.doi.org/10.1016/j.combustflame.2016.03.031.

[9] R. Payri, J.P. Viera, V. Gopalakrishnan, P.G. Szymkowicz, The effect of nozzle geometry over the evaporative spray formation for three different fuels, Fuel 188 (2017) 645–660, http://dx.doi.org/10.1016/j.fuel.2016.06.041.

[10] C. Sayin, M. Gumus, M. Canakci, Influence of injector hole number on the performance and emissions of a di diesel engine fueled with biodiesel-diesel fuel blends, Appl. Therm. Eng. 61 (2013) 121–128, http://dx.doi.org/10.1016/j.applthermaleng.2013.07.038.

[11] G. Aori, D.L.S. Hung, M. Zhang, Effect of nozzle configuration on macroscopic spray characteristics of multi-hole fuel injectors under superheated conditions, Atomization Spray 26 (2016) 439–462, http://dx.doi.org/10.1615/AtomizSpr.2015011990.

[12] L.Y. Zhou, S.F. Dong, H.F. Cui, X.W. Wu, F.Y. Xue, F.Q. Luo, Measurements and analyses on the transient discharge coefficient of each nozzle hole of multi-hole diesel injector, Sensor Actuat. A-Phys. 244 (2016) 198–205, http://dx.doi.org/10.1016/j.sna.2016.04.017.

[13] C. Chartier, U. Aronsson, Ö. Andersson, R. Egnell, B. Johansson, Influence of jet-jet interactions on the lift-off length in an optical heavy-duty DI diesel engine, Fuel 112 (2013) 311–318, http://dx.doi.org/10.1016/j.fuel.2013.05.021.

[14] A.M. Rusly, M.K. Le, S. Kook, E.R. Hawkes, The shortening of lift-off length associated with jet-wall and jet-jet interaction in a small-bore optical diesel engine, Fuel 125 (2014) 1–14, http://dx.doi.org/10.1016/j.fuel.2014.02.004.

[15] R.S.G. Baert, P.J.M. Frijters, B. Somers, C.C.M. Luijten, W.D. Boer, W. de Boer, Design and operation of a high pressure, high temperature cell for HD diesel spray diagnostics: guidelines and results, SAE Trans. 4970 (2009) http://dx.doi.org/10.4271/2009-01-0649.

[16] M. Bardi, R. Payri, L.-M. Malbec, G. Bruneaux, L.M. Pickett, J. Manin, T. Bazyn, C.L. Genzale, Engine combustion network: Comparison of spray development, vaporization, and combustion in different combustion vessels, Atomization Spray 22 (2012) 807–842, http://dx.doi.org/10.1615/AtomizSpr.2013005837.

[17] C. Zhang, Y. Wu, B. Liu, Z. Wang, L. Zhou, Investigation of soot particles morphology and size distribution produced in a n-heptane/anisole laminar diffusion flame based on TEM images, Combust. Flame 244 (2022) 112234, http://dx.doi.org/10.1016/j.combustflame.2022.112234.

[18] H.S. Sim, N. Maes, L.M. Pickett, S.A. Skeen, J. Manin, High-speed formaldehyde planar laser-induced fluorescence and schlieren to assess influences of injection pressure and oxygen concentration on Spray A flames, Combust. Flame 253 (2023) 112806, http://dx.doi.org/10.1016/j.combustflame.2023.112806.

[19] M.K. Le, Y. Zhang, R. Zhang, L. Rao, S. Kook, Q.N. Chan, E.R. Hawkes, Effect of jet-jet interactions on soot formation in a small-bore diesel engine, P Combust. Inst. 36 (2017) 3559–3566, http://dx.doi.org/10.1016/j.proci.2016.07.025.

[20] G. Lequien, E. Berrocal, Y. Gallo, A.T.E. Mello, O. Andersson, B. Johansson, Effect of jet-jet interactions on the liquid fuel penetration in an optical heavy-duty DI diesel engine, in: SAE Technical Papers, vol. 2, SAE International, 2013, http://dx.doi.org/10.4271/2013-01-1615.

[21] C.J. Polonowski, C.J. Mueller, C.R. Gehrke, T. Bazyn, G.C. Martin, P.M. Lillo, An experimental investigation of low-soot and soot-free combustion strategies in a heavy-duty, single-cylinder, direct-injection, optical diesel engine, SAE Int. J. Fuels Lubr. 5 (2011) 51–77.

[22] L.M. Malbec, G. Bruneaux, Study of air entrainment of multi-hole diesel injection by particle image velocimetry-effect of neighboring jets interaction and transient behavior after end of injection, SAE Tech. Pap. 3 (2010) 107–123, http://dx.doi.org/10.4271/2010-01-0342.

[23] T. Fuyuto, Y. Hattori, H. Yamashita, N. Toda, M. Mashida, Set-off length reduction by backward flow of hot burned gas surrounding high-pressure diesel spray flame from multi-hole nozzle, Int. J. Engine Res. 18 (2017) 173–194, http://dx.doi.org/10.1177/1468087416640429.

[24] T. Bazyn, C. Koci, The effect of jet spacing on the combustion characteristics of diesel sprays, in: THIESEL 2014 Conference on Thermo- and Fluid Dynamic Processes in Direct Injection Engines, Valencia (Spain), 2014, pp. 1–19.

[25] R. Payri, J. Gimeno, M. Carreres, T. Montiel, Understanding the effect of inter-jet spacing on lift-off length and ignition delay, Combust. Flame 230 (2021) http://dx.doi.org/10.1016/j.combustflame.2021.111423.

[26] J. Manin, L.M. Pickett, S.A. Skeen, Two-color diffused back-illumination imaging as a diagnostic for time-resolved soot measurements in reacting sprays, SAE J-Automot. Eng. 6 (2013) 1908–1921, http://dx.doi.org/10.4271/2013-01-2548.

[27] R. Payri, J. Gimeno, S. Cardona, S. Ayyapureddi, Experimental study of the influence of the fuel and boundary conditions over the soot formation in multi-hole diesel injectors using high-speed color diffused back-illumination technique, Appl. Therm. Eng. 158 (2019) 113746, http://dx.doi.org/10.1016/J.APPLTHERMALENG.2019.113746.

[28] R. Payri, F.J. Salvador, J. Gimeno, G. Bracho, The effect of temperature and pressure on thermodynamic properties of diesel and biodiesel fuels, Fuel 90 (2011) 1172–1180, http://dx.doi.org/10.1016/j.fuel.2010.11.015.

[29] J. Gimeno, P. Martí-Aldaraví, M. Carreres, J.E. Peraza, Effect of the nozzle holder on injected fuel temperature for experimental test rigs and its influence on diesel sprays, Int. J. Engine Res. 19 (2018) 374–389, http://dx.doi.org/10.1177/1468087417751531.

[30] R. Payri, P. Martí-Aldavarí, T. Montiel, A. Viera, Influence of aging of a diesel injector on multiple injection strategies, Appl. Therm. Eng. 181 (2020) 115891, http://dx.doi.org/10.1016/j.applthermaleng.2020.115891.

[31] R. Payri, J. Gimeno, P. Martí-Aldavarí, T. Montiel, Influence of the inter-jet spacing of diesel sprays on the combustion development, in: ICLASS 2021, 15th Triennial International Conference on Liquid Atomization and Spray Systems, Edinburgh, UK, 2021, pp. 1–8, http://dx.doi.org/10.2218/iclass.2021.5987.

[32] S.S. Pandurangi, M. Bolla, Y.M. Wright, K. Boulouchos, S.A. Skeen, J. Manin, L.M. Pickett, Onset and progression of soot in high-pressure n - Dodecane sprays under diesel engine conditions, Int. J. Engine Res. 18 (2017) 436–452, http://dx.doi.org/10.1177/1468087416661041.

[33] J. Manin, M. Bardi, L.M. Pickett, R.N. Dahms, J.C. Oefelein, Microscopic investigation of the atomization and mixing processes of diesel sprays injected into high pressure and temperature environments, Fuel 134 (2014) 531–543, http://dx.doi.org/10.1016/j.fuel.2014.05.060.

[34] R. Payri, G. Bracho, P. Marti-Aldaravi, A. Viera, Near field visualization of diesel spray for different nozzle inclination angles in non-vaporizing conditions, Atomization Spray 27 (2017) 251–267, http://dx.doi.org/10.1615/AtomizSpr.2017017949.

[35] J.V. Pastor, J.M. García-Oliver, C. Micó, A.A. García-Carrero, A. Gómez, Experimental study of the effect of hydrotreated vegetable oil and oxymethylene ethers on main spray and combustion characteristics under engine combustion network spray a conditions, Appl. Sci. 10 (2020) http://dx.doi.org/10.3390/APP10165460.

[36] J. Manin, L.M. Pickett, S.A. Skeen, Toward quantitative spray measurements using high-performance high-speed video cameras, in: ILASS Americas 2016, Mighigan, USA, 2016, pp. 511–518.

[37] J.V. Pastor, J.M. Garcia-Oliver, R. Novella, T. Xuan, Soot quantification of single-hole diesel sprays by means of extinction imaging, SAE J-Automot. Eng. 8 (2015) 2068–2077, http://dx.doi.org/10.4271/2015-24-2417.

[38] G. Farnebäck, Two-frame motion estimation based on polynomial expansion, Lect. Notes Comput. Sc 2749 (2003) 363–370, http://dx.doi.org/10.1007/3-540-45103-x_50.

[39] J.V. Pastor, A. García, C. Micó, A.A. García-Carrero, Experimental study of influence of liquefied petroleum gas addition in hydrotreated vegetable oil fuel on ignition delay, flame lift off length and soot emission under diesel-like conditions, Fuel 260 (2020) 116377, http://dx.doi.org/10.1016/j.fuel.2019.116377.

[40] M.Y. Choi, G.W. Mulholland, A. Hamins, T. Kashiwagi, Comparisons of the soot volume fraction using gravimetric and light extinction techniques, Combust. Flame 102 (1995) 161–169, http://dx.doi.org/10.1016/0010-2180(94)00282-W.

[41] Ü.Ö. Köylü, C.S. Mcenally, D.E. Rosner, L.D. Pfefferle, Simultaneous measurements of soot volume fraction and particle size / microstructure in flames using a thermophoretic sampling technique, Combust. Flame 110 (1997) 494–507, http://dx.doi.org/10.1016/S0010-2180(97)00089-8.

[42] J.M. Desantes, J.M. García-Oliver, A. García, T. Xuan, Optical study on characteristics of non-reacting and reacting diesel spray with different strategies of split injection, Int. J. Engine. Res. 20 (2019) 606–623, http://dx.doi.org/10.1177/1468087418773012.

[43] R. Payri, F.J. Salvador, J. Manin, A. Viera, Diesel ignition delay and lift-off length through different methodologies using a multi-hole injector, Appl. Energ. 162 (2016) 541–550, http://dx.doi.org/10.1016/j.apenergy.2015.10.118.

[44] T. Li, H. Ogawa, Analysis of the trade-off between soot and nitrogen oxides in diesel-like combustion by chemical kinetic calculation, SAE J-Automot. Eng. 5 (2011) http://dx.doi.org/10.4271/2011-01-1847.